The Birth of Gravitational Wave Astronomy

Mainak Singha

University College Dublin

A thesis submitted under the supervision of Prof. Adrian Ottewill for the degree of

Master of Space Science and Technology

Dublin 2016

This thesis is specially dedicated to

my loving parents and my beloved Elena

who never left my side

Acknowledgements

Firstly, I might want to express my true appreciation to my supervisor Prof.Adrian Ottewill for the persistent support throughout the research, for his understanding, inspiration, and valuable information. His direction helped me in all the time of research and composing this thesis. I couldn't have envisioned having a superior supervisor and guide for my task.

My true thanks additionally goes to Dr.Barry Wardell, who gave me a chance to join their group as an intern, and who offered access to the exploration to all the research facilities. Without his valuable bolster it would not be conceivable to direct this research.

Last but certainly not the least, I would like to thank my loving parents, and my beloved Elena for supporting me profoundly all through composing this thesis and my life.

Abstract

What is a Gravitational Wave? It is the ripples in the curvature of space-time propagating as waves. It has not been detected for a long time since its strain amplitude is extremely low and the detectors were not sensitive enough. Thanks to LIGO that their detectors have been sensitive enough to detect it. Here, a matched filtering analysis have been performed to investigate the truth about the detection, where the strain data from the two interferometers have been whitened and filtered using bandpass and notch filter. It ultimately gets matched with the NR template very well. A good way to search for a gravitational wave is performing a blind burst search where the signal. Here, the the signal has shown some properties which also has confirmed the detection of gravitational wave as well. There are three phases for the event- inspiral, merger, ringdown among which the merger and the ringdown is still not clear. When their relativistic motion begins only one approach can successfully explain the whole scenario- 'Effective One Body' formalism. Here it explains a lot about the last stages of inspiral and the merger. To understand the ringdown phase an easy but effective way is to comapre it with a similar looking signal model. The dominant QNM ringdown frequency is the frequency of the least damped part. It has been determined with the frequency equation of ringdown phase and the analytical value gets very well matched with the observed wave. In the low frequency domain ($\approx$ 1 Hz) classical mechanics holds good . So, applying simple physics for compact binaries it is possible to predict the existence of gravitational wave in that domain.

Contents

List of Figures

Chapter 1

A matched filtering analysis of LIGO data

1.1 How do the interferometer data actually look like?

GW150914 was a major breakthrough in the history of 'Gravitational Wave Astronomy'. It was the first and foremost sound proof of the existence of the gravitational wave. The false alarm rate is estimated to be less than 1 event per 203,000 years, which is said to be equivalent to a significance of 5.1 sigma. The event was detected in the detectors of the LIGO observatories at LIGO Hanford and LIGO Livingston in the United States.

But the question arises is how the actual raw data looks like? Well, they actually do not look that good because they are highly dominated by the background noise. So, the signal is almost well-hidden inside the noise. If a spectrogram of the raw data is taken a faint patch will be visualised. In the next chapter ,this topic has been discussed in detail. But for the time being let us have a look how the data from the 2 observatories actually look like

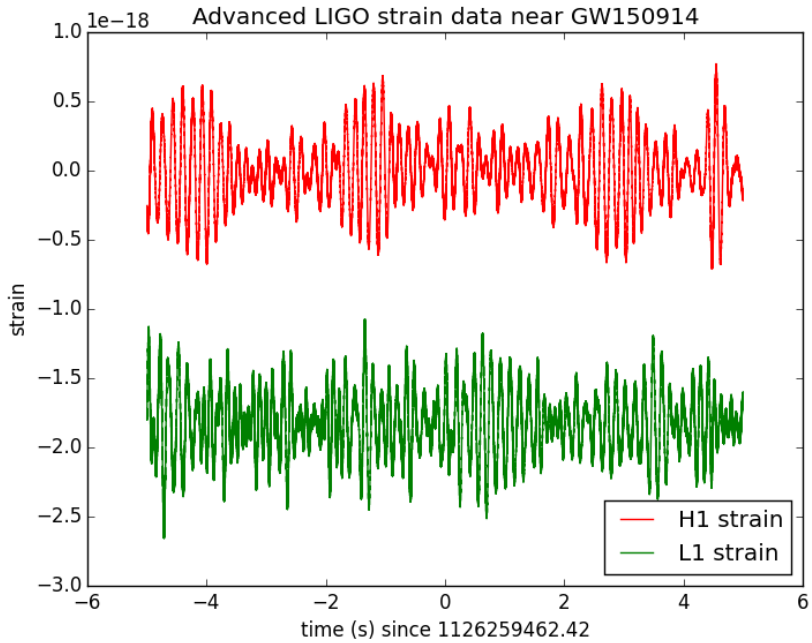

Figure 1.1: aLIGO Hanford and Livingston raw strain data

1.2 Generating the GW waveform from SXS templates

The application of numerical relativity has been magnificently handy when it comes down to gravitational wave astronomy. One of its greatest gift is to construct the template of GW from a BBH coalescence. Such templates are available on the SXS page containing SpEC waveforms which are provided at so many fixed extraction radii and along with that they are extrapolated to different extrapolation orders (N=2,3,4). Thy are also in different resolutions. For the best result we shall work with the top resolution data file. Numerical accuracy can be assessed from the difference between different numerical resolutions. For runs with only a single resolution, look at a similar run. (Precession does not change numerical accuracy of our runs, but different mass ratios and spin magnitudes do).

We shall focus on the dominant "Quasi Normal Mode" (QNM) is the (l=2,m=2)

mode. It indicates the direction where the signal is the strongest or the direction. And the mass ratio is 1.2484. The nearest mass ratio available on the template is 1.26.

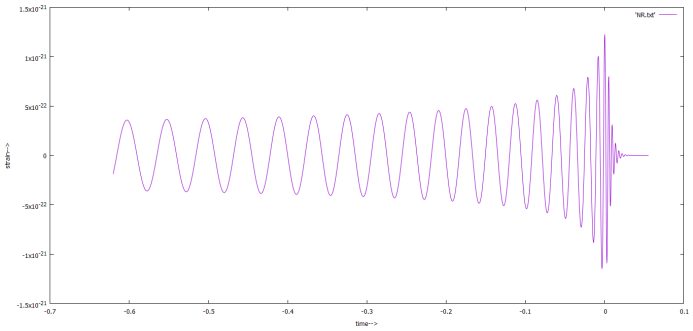

Figure 1.2: NR waveform

The technique of matched filtering analysis is as follows - firstly, a waveform will be generated using the templates. Next, the strain data will be filtered to find the signal. If finally, the waveforms from both the Handford and Livingston detectors fits with the template waveform then only we can be assured that we have detected 'Gravitational Wave'.

1.3 Computing ASD of the data

If we plot these data in the fourier domain it will give us a decent amount of idea of the frequency content in the aforementioned data. A great way to envision this scenario is plotting the 'Amplitude Spectral Density' or simply ASD, which is simply the square root of the Power Spectral Densities (PSDs) known to be the averages of the square of the FFT (Fast Fourier Transform) of the data. These can be said to be a brief estimate of the "Strain-Equivalent Noise" of the LIGO detectors versus frequency, limiting the LIGO detectors' ability in identifying the 'Gravitational Wave' (GW) signals. Those data are in the units of strain/rt(Hz) In order to determine the root-mean-square (rms) strain noise in a frequency band, we have to just integrate

(sum) the squares of the ASD over that band, followed by taking the square-root. Although there is a GW signal here in the dataset, for the time being lets us consider that it is nothing but just noise.

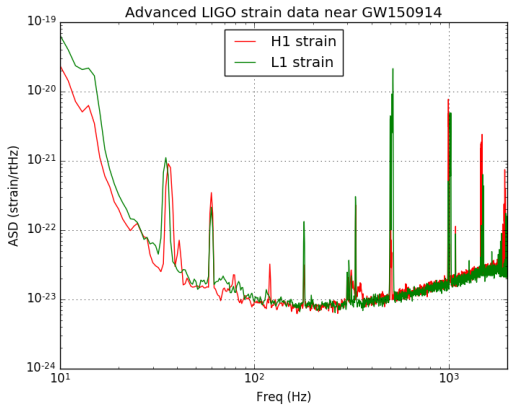

Figure 1.3: ASD of GW150914

Here the plot is mainly between frequency range 10-2000 Hz where $f_{min} = 10Hz$ and $f_{max} = 2000Hz$. If we go below f_{min} we'll find that the data is not properly calibrated.

That is reasonable due to high noise that the LIGO detectors is unable to sense gravitational wave strain from the "Binary Black Holes" (BBH) or other astrophysical sources. Here the sample rate is $f_s = 4096Hz$ which is basically 2^12Hz for that reason the data is unable to capture any sort of frequency content above the 'Nyquist Frequency $= f_s/2 = 2048Hz$. That is because GW150914 consists of frequency content in the frequency range 20-300 Hz.

"Strong spectral lines in the data are visible; they are all of instrumental origin. Some are engineered into the detectors and some are unwanted. The signal in this plot is not visible, since it is not strong and almost less than a second long, while this plot averages over 32 seconds of data. So this plot is entirely dominated by instrumental noise".

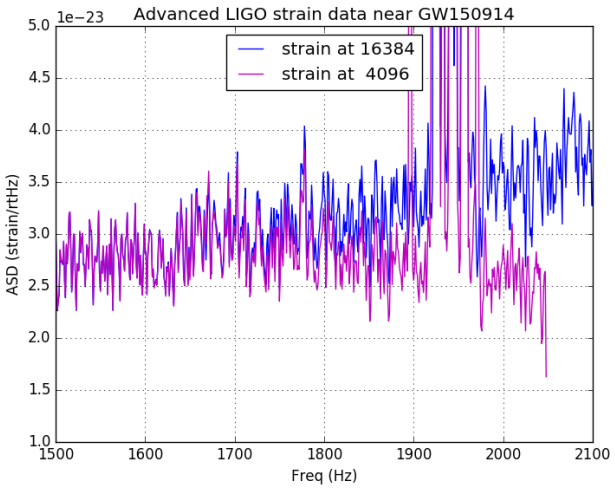

Figure 1.4: Zoomed ASD of GW150914

1.4 Whitening the GW150914 data

In the ASD we have just plotted above, it is clearly visible that the data are extremely strongly "coloured" - the noise fluctuations are significantly large at the low and high frequency domains and in vicinity of the spectral lines, reaching a approximately flat ("white") minima in the band around 80 to 300 Hz. It is possible for us to whiten the data which is basically dividing it by the noise amplitude spectrum, in the fourier domain which will suppress the extra amount of noise at the low frequency domain and at the spectral lines as well, for a better visualisation of the weak signals in the most sensitive field as well.

While analysing any astrophysical data (searches, estimating parameters), whitening is always considered to be the first step. For this purpose only the data is needed. Another important thing is, the resulting time series will be no longer in the 'strain' units, but in the units of 'sigmas' away from the mean.

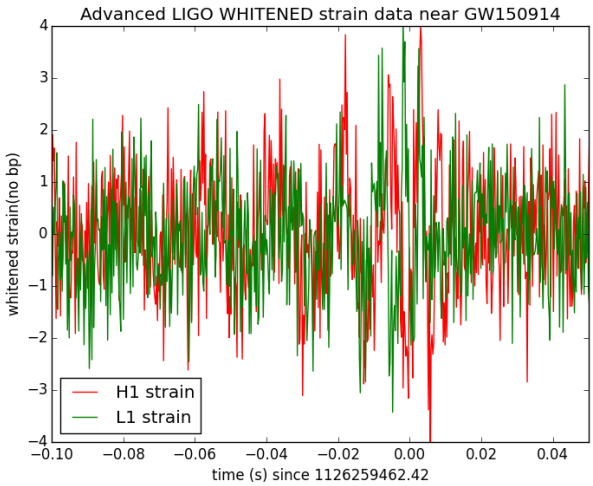

Figure 1.5: ASD of GW150914 whitened data

1.5 Filtering the GW150914 data

To visualise the signal it is extremely essential to filter the data. For the purpose we are going to use two different to get rid of the noise as much as we can so to recognise the signal properly. In signal processing, a filter is said to be a process which is capable of removing some unwanted components/ features from a signal. Filtering is typically a type of 'signal processing', the motivation behind defining feature of filters is to completion or 'partial suppression of some aspect of the signal'. Often, it implies removing some frequencies and not others for suppressing the interfering signals and to reduce the background noise as much as possible. Here we shall be using the bandpass filter and the bandstop or notch filter.

For the bandpass filter the parameters are as lowcut = 43 Hz, highcut = 260 Hz and order = 4. We shall manually construct a wider notch filter around the frequency 510 Hz. Furthermore, our goal will be to notch out the forest of lines around the frequency 331.5 Hz as well.

With the help of the moving puncture technique (considering black hole as a puncture in the space-time, along with the gauge evolution together with the "fourth-order Runge-Kutta time integration", "fourth-order accurate finite spatial differencing",

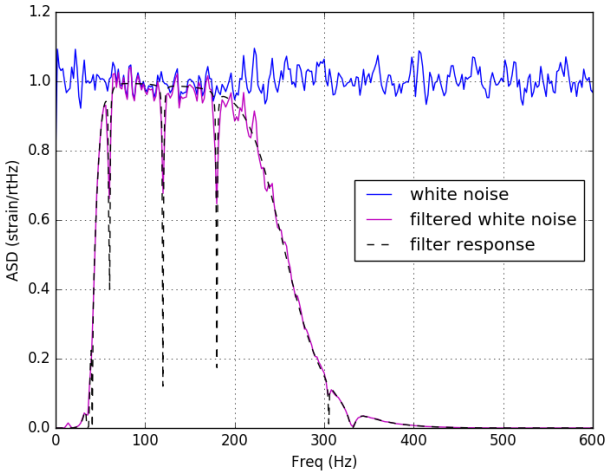

Figure 1.6: Filter response

and second-order-accurate initial data", we can simulate the GW of the LIGO BBH system getting started at a significantly large separation or 6 orbits before the common event horizon formation. And with the help of this technique, that previous strain data now looks like this

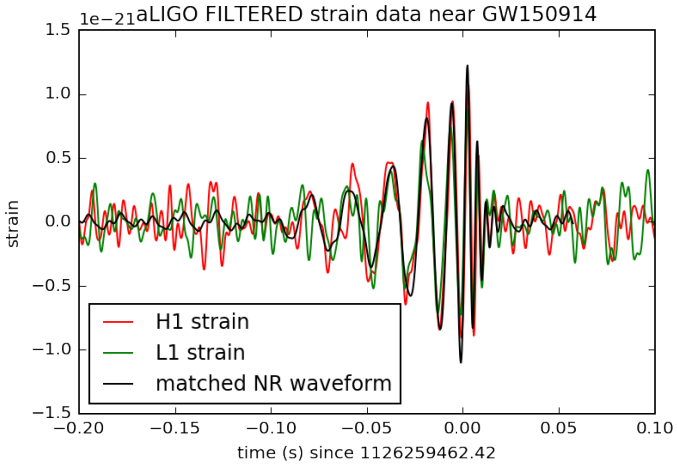

Figure 1.7: Filtered aLIGO strain data

And finally we found this (plot down below), that the both Hanford and Livingston data getting completely matched extremely well with each other and with the one generated with numerical relativity which clears all doubt. So, we can finally say that, we have detected 'Gravitational Wave'.

Chapter 2

A Bind Burst search in search of the Gravitational Waves

2.1 Search for Gravitational Wave Burst

Strain data are sought by gravitational wave burst search algorithms' without accepting a specific sign morphology, cause, direction or time. Burst searches are performed in two operational modes; on-line and off-line. On-line, 'low-latency search' give alarms inside minutes of a gravitational wave signal passing the detectors to encourage follow-up investigations, for example, scanning for electromagnetic partners. In the days and weeks taking after the information gathering, burst investigations are refined utilising updated data on the information quality and calibrating detectors to perform off-line searches. These off-line searches give enhanced identification certainty assessments to GW applicants, measure sensitivity, and add to waveform recreation and astrophysical elucidation.

2.2 Coherent Wave Burst

The cWB calculation has been utilised to play out all-sky searches for gravitational wave transients in LIGO. The cWB calculation has subsequent to been moved up to direct transient searches with the advanced detectors. The cWB pipeline was utilised as a part of the low-latency transient hunt that at first recognised GW150914, reporting the occasion three minutes after the information was gathered. This quest goes for quick alarms for the LIGO electromagnetic followup program and gives a first estimation of the occasion parameters and sky location. A marginally diverse setup of the same pipeline was utilised as a part of the off-line pursuit to gauge the factual importance of the GW150914 occasion. The lowlatency hunt was performed in the frequency range of 16-2048 Hz, while the off-line search secured the band of the sensitivity of the best detector somewhere around 16 and 1024 Hz.

2.2.1 cWB pipeline overview

he cWB pipeline hunts down an expansive scope of gravitational wave transients in the LIGO frequency band without earlier learning of the signal waveforms. The pipeline recognises incidental occasions in information from the two LIGO detectors and remakes the gravitational wave signal connected with these occasions utilising a probability examination.

In the first place, the information are whitened and changed over to the time-frequency space utilising the Wilson-Daubechies-Meyer wavelet change. Information from both identifiers are then joined to get a time-frequency power map. A transient occasion is distinguished as a group of time-frequency information tests with force over the pattern identifier commotion. To acquire a decent time-frequency scope for an expansive scope of sign morphologies, the investigation is rehashed with seven frequency resolutions f extending from 1 Hz to 64 Hz in ventures of forces of two,

comparing to time resolutions

$$Vt = 1/(2\Delta f)$$

from 500 ms to 7.8 ms. The bunches at various resolutions covering in time and frequency are joined into a trigger that gives a multi-resolution representation of the excessive power events recorded by the detectors.

The information connected with every trigger are investigated intelligibly [24] to appraise the signal waveforms, the wave polarisation, and the source sky area. The signal waveforms in both identifiers are reproduced with the obliged probability strategy. The imperative utilised as a part of this investigation is model autonomous and requires the remade waveforms to be comparative in both detectors, not surprisingly from the nearby arrangement of the H1 and L1 finder arms. The waveforms are recreated over a uniform lattice of sky areas with 0.4×0.4 determination. We select the best fit waveforms that compare to the greatest of the probability measurement.

$$L = c_c E_s$$

where E_s is the aggregate vitality of the reproduced waveforms1 and cc measures the comparability of the waveforms in the two finders. The coefficient cc is characterised as

$$c_c = E_c/(E_c + E_n)$$

where E_c is the normalised coherent energy and En is the normalised energy of the residual noise after the remade signal is subtracted from the information. E_c is corresponding to the cross-connection between the remade signal waveforms in H1 and L1 identifiers. Commonly, gravitational wave signs are cognisant and have little lingering vitality i.e., E_c, E_n and along these lines $c_c 1$. Then again, spurious

commotion occasions (glitches) are frequently not intelligible, and have substantial leftover vitality in light of the fact that the remade waveforms don't fit well the information i.e., E_c, E_n and along these lines c_c. The positioning measurement is characterised as

$$\eta_c = (2c_c E_c)^{1/2}$$

By development, it favours gravitational-wave signals related in both detectors.

2.2.2 Classification of cWB events

Events produced by the cWB pipeline with $c_c > 0.7$ are chosen and separated into three classes C1, C2, and C3 as indicated by their time-frequency morphology. The motivation behind this occasion grouping is to represent the non-Gaussian noise that happens non-consistently over the parameter space sought by the pipeline. The classes are controlled by three algorithmic tests and extra determination cuts. The primary algorithmic test addresses a particular sort of noise transient alluded to as "blip glitches". Amid the run, both detectors experienced noise transients of obscure inception comprising of a couple cycles around 100 Hz. These blip glitches have an extremely trademark time-symmetric waveform with no unmistakable frequency evolution. Past work has demonstrated that down-weighting signals with straightforward time-frequency structure can improve pipeline execution.

To actualise this here, we apply a test that utilise waveform properties to distinguish, in the time area, blip glitches happening at both detectors. The second algorithmic test distinguishes glitches due to non-stationary tight band elements, for example, power and mechanical reverberation lines. This test chooses hopefuls which have the vast majority of their vitality (more noteworthy than 80 percent) restricted in a frequency transmission capacity under 5 Hz. A cWB occasion is put in the enquiry

class C1, on the off chance that it breezes through both of the previously mentioned tests. What's more, because of the raised non-stationary commotion around and beneath the Progressed LIGO mechanical resonances at 41 Hz, occasions with focal recurrence lower than 48 Hz were additionally set in the C1 class.

The third algorithmic test is utilised to distinguish occasions with a recurrence expanding with time. For signals that don't start from combining parallels and glitches, M goes up against unphysical values. In the un-displayed cWB investigation, the parameter M is utilised to recognise occasions with various time-frequency evolution. By selecting occasions with $M > 1M_s$ tweeting time-frequency signature, which incorporates a subclass of blending double flags. The occasions chose by this test likewise have a lingering vitality En reliable with Gaussian commotion are set in the hunt class C3. Every single other event, excluded into the C1 or C3 class, are put in the class C2. The union of every one of the three free hunt classes covers the full parameter space open to the unmodelled cWB seek.

2.2.3 False alarm rate

In order to set up the distribution of background events, we utilise the time-shift methodology utilising every one of the information accessible for every detector. The viable foundation livetime for this examination is 67 400 years, acquired by breaking down more than 1.6 106 time-shifted occurrences of 16 days of the perception time. The hugeness of a candidate event is measured against the foundation of its class. The C1 seek class is influenced by a tail of blip glitches with the false alert rate of roughly 0.01 per year.

Con-fining glitches in the C1 class upgrades the enquiry affectability to gravitational-wave signals falling in the C2 and C3 classes. Truth be told, the tail is decreased by more than two requests of extent in the C2 look class. The foundation rates in the C3 seek class are very nearly ten times lower than in C2, with no conspicuous tail of

uproarious occasions, demonstrating that it is exceptionally improbable for identifiers to create sound foundation occasions with a twittering time-recurrence advancement.

2.2.4 Significance of GW150914

GW150914 was distinguished with $\eta_c = 20$ and has a place to the C3 class. Its η_c worth is bigger than the identification measurement of all watched cWB applicants. The GW150914 η_c quality is bigger than the discovery measurement of any background event in its class in 67400 years of the comparable perception time. All other watched occasion hopefuls are reliable with the background. The GW150914 significance is characterised by its false caution rate measured against the foundation in the C3 class. Expecting that all classes are factually free, this false alert rate ought to be expanded by a traditionalist trial variable equivalent to the quantity of classes. The assessed GW150914 false alert rate is short of what one occasion in 22500 years. The likelihood that the 16 days of information would yield a noise event with this false caution rate is less than $16/(36522500) = 2 \times 10^{-6}$.

The union of the C2 and C3 look classes speaks to a transient hunt without any presumptions on the sign time-frequency development. For this situation there are four occasions louder than GW150914 in the C2 + C3 class. With the trials variable of 2, the false alert rate is one occasion in 8400 years. The four boisterous occasions are delivered by an irregular incident of numerous blip glitches: two close-by blip glitches in one detector and a solitary blip glitch in the second indicator. The algorithmic test that distinguishes blip glitches was most certainly not intended to catch numerous ones and, along these lines, missed these occasions.

Here the spectrogram of the Hanford data has been plotted. About the blind search and false alarm rate has been mentioned earlier. Then how did we confirm it is the true signal? The time difference for the signal between Hanford and Livingston was 7 ms which is the exact time taken by gravitational wave to travel the required

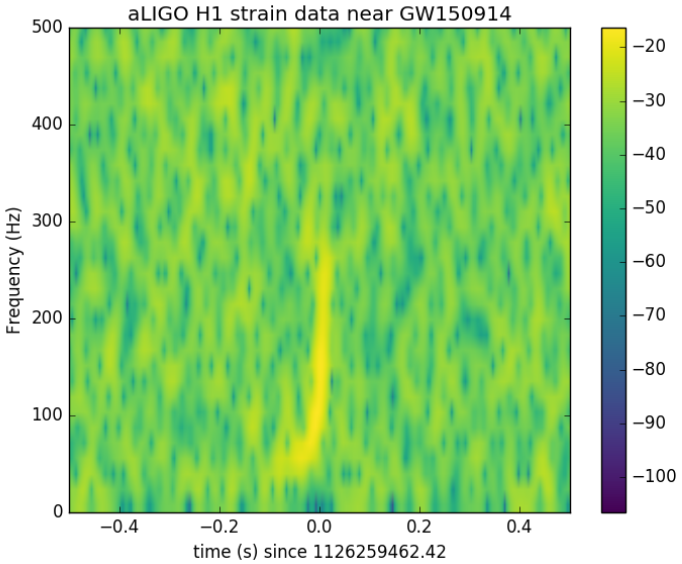

Figure 2.1: The Spectrogram of the Hanford strain data. The smudge between -0.2 to 0 s is the signal

distance. As for the burst search, it is seen that the signal clearly stands out from the background. All these give us a proper evidence of the detection.

2.3 Search for sources

2.3.1 Source localisation

Here, we look at cWB, LIB, and BayesWave skymaps notwithstanding the guide delivered by LALInference with paired combination layouts, which tests the back circulation of every single sign parameter utilising signal waveforms that cover the inspiral, merger and ringdown stage . LIB utilises a space of single sine-Gaussian waveforms as its waveform model, and delivers skymaps following one to two hours, while BayesWave maps can take the length of a few days to be created, since it investigates a bigger parameter space of superpositions of sine-Gaussian waveforms. Blasted confinement calculations create methodically bigger skymaps than layout based calculations since they make less presumptions about the waveform. For GW150914,

we anticipate that the LALInference guide will yield a moderately exact restriction, since it expect a waveform from a smaller paired combination, rather than the wide waveform classes utilised by the burst pipelines.

2.3.2 Parameter estimation

The source parameters of GW150914, for example, part masses and spins, can be very much portrayed by utilising an expository model of BBH signs to register their back dissemination . Here, we take an alternate methodology, which utilises the yields of the burst pipelines to give a coarse assessment of the model parameters. The BayesWave and cWB waveform recreations can be used to register an assortment of parameters that abridge the signal, for example, the central frequency, term what's more, transfer speed. These parameters can then be utilised to identify qualities of the astrophysical framework that produced the sign. Utilising waveform formats for a BBH merger, we can determine forecasts for the central frequency and data transmission of the sign in every detector as an element of the mass, mass proportion and spins.the best portrayal of this sign yields an indicator outline complete mass of $M = 71^{+5}_{-4} M_s$ and a mass proportion of $q = 0.82^{+0.17}_{-0.20}$. Applying the same system to the 29 GW150914-like hardware injections we found that the central frequency what's more, transmission capacity of the infused signals fell inside the half believable interim half of the time, and inside the 90 percent believable interim 89 percent of the time, demonstrating that the search is reliable.

2.3.3 Detection of chirp mass

The cWB pipeline acquires the time-frequency templates of the events by utilising a discrete wavelet change. Given an example with N time-recurrence segments $(t_i, f_i), i = 1, , N$ from a mixing twofold, at the main postNewtonian request it is portrayed when frequency evolution. The constant search that initially identified

GW150914 evaluated its detector outline chirp mass to be $27.62.0M_s$.This outcome is steady with the LALInference assessment of $30^{+2}_{-2}M_s$.

To check the precision of the constant strategy, we concentrated on 29 equipment infusions with parameters like those deduced for GW150914. We found that this technique could precisely remake the peep masses of these mimicked signals, with an accuracy like the cited instability.

2.3.4 Overlap between reconstructed waveform and BBH model

By contrasting the NR waveforms, which spread areas of the parameter space which are not as a matter of course all around displayed and incorporate higher sounds, with the model-free reproduced waveforms which can recuperate the full astrophysical sign substance, we are delicate to takeoffs from both the logical layouts utilised somewhere else and from the forecasts of general relativity.

Contrasting straightforwardly with NR waveforms permits us to investigate locales of parameter space where the diagnostic formats have not yet been tuned, for example, very precessing turn designs and their higher music. Truth be told, we find magnificent similarity between this study and the parameter estimation performed with explanatory layouts, and in addition with the parameter estimation strategy utilising just NR waveforms which is accounted for.

Chapter 3

The dominant QNM ring down frequency

3.1 Testing for the least damped Quasi Normal Mode

We perform a test to check the consistency of the data with the predicted least-damped QNM of the remnant black hole. For this purpose we compute the Bayes factor between a damped sinusoid waveform model and Gaussian noise, and estimate the corresponding parameter posteriors. The signal model used is

$$h(t \geq t_0) = Ae^{-(t-t_0/\tau)}cos2\pi f_0((t-t_0)+\phi_0) \ ,$$

$h(t < t_0) = 0$, with altered beginning time t_0, and uniform priors over the obscure frequency f_0 ranges from 200 to 300 Hz and damping time τ ranges from 0.5 to 20 ms. The prior on amplitude A and stage ϕ_0 is picked as a two-dimensional Gaussian isotropic earlier in $A_s Asin\phi_0, A_c Acos\phi_0$ with a characteristics scale H, which is thusly underestimated over the range $H \in [2, 10]10^{22}$ with an earlier $\propto 1/H$.

This is a useful decision that encodes relative obliviousness about the discernible damped-sinusoid adequacy in this reach. We utilise 8s of information (fixated on GW150914) from both detectors, band-went to the range [20, 1900] Hz. The information are investigated rationally, accepting the sign arrived 7 ms before at Livingston contrasted with Hanford, and the adequacy got in the two detectors has roughly rise to greatness and inverse sign. We compute the Bayes factor and back evaluations of f_0, τ as an element of the obscure QNM begin time t_0, which we parametrise as a counterbalance from a fiducial GPS merger time3 $t_M = 1,126,259,462.423s$

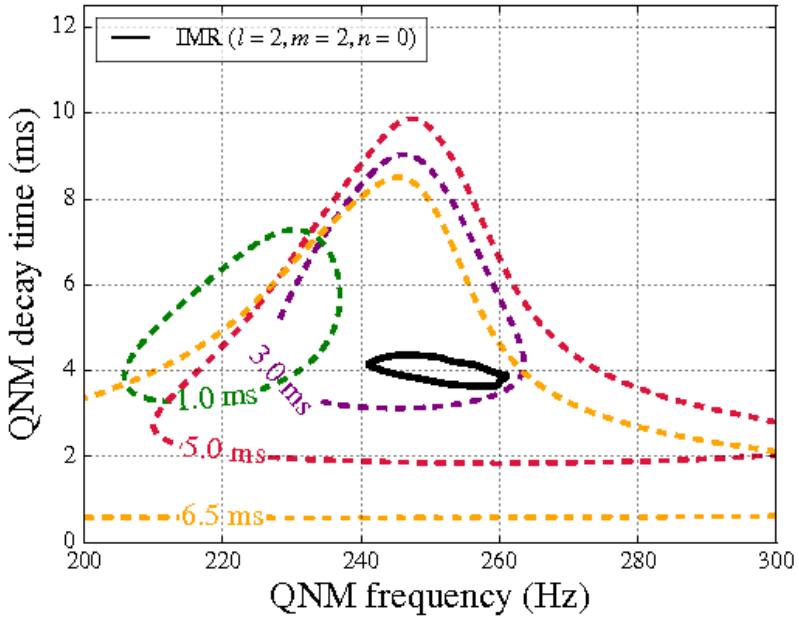

Figure 3.1: 90 percent credible regions in the joint posterior distributions for the damped-sinusoid parameters

The figure above demonstrates the contours that fall into the credible category the f_0, plane as a component of the merger-to-starter time counterbalance t0 tM, and in addition, the relating form for the slightest damped QNM as anticipated in GR for the remainder mass and turn parameters evaluated for GW150914.

The 90 percent back shape begins to cover with GR prediction from the IMR waveform for $t_0 = t_M + 3$ ms, or 10 M after merger. The comparing log Bayes component now is log10 B 14 and the MAP waveform SNR is 8.5. For $t_0 = t_M + 5$

ms the MAP parameters fall inside the form anticipated in GR for the slightest damped QNM, with $log_{10}B = 6.5$ and SNR $= 6.3$. At $t_0 = t_M + 6.5$ms, or around 20 M after merger, the Bayes variable is$log_{10}B = 3.5$ with SNR $= 4.8$. The sign gets to be imperceptible presently, for $t_0 \geq t_M + 9$ ms for $B \leq 1$.

Measuring the frequency and decay time of one damped sinusoid in the information does not without anyone else permit us to infer that we have watched the minimum damped QNM of the last dark opening, following the deliberate quality element could be one-sided by the nearness of alternate QNMs in the ringdown signal . Be that as it may, in light of the numerical recreations, one ought to anticipate that the GW frequency will level off at 10 20 M after the merger, which is the place the portrayal of ringdown as far as QNMs gets to be legitimate.

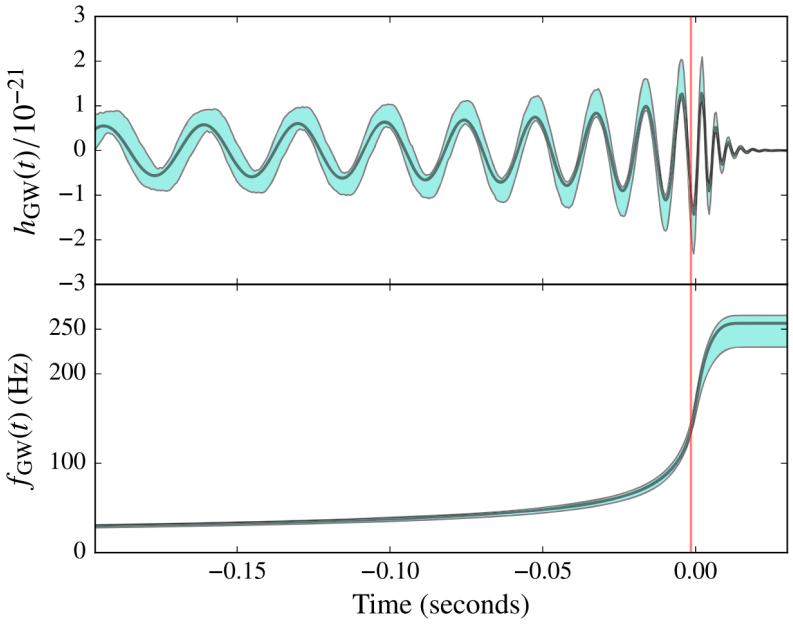

Figure 3.2: The waveform of gravitational wave and the time variation of the frequency

For a mass $M = 68M_s$, the corresponding range is almost 3 -7 ms after merger. Since this is the place we watch the 90 percent back shapes of the damped sinusoid waveform model and the 90 percent confidence region evaluated from the IMR waveform to be reliable with each other, we may presume that the information are perfect with the nearness of the slightest damped QNM as anticipated by GR.

3.2 Determining the dominant ringdown frequency

In order to describe the ringdown phase we take help of quite a few assumptions. The first one is the least damped stage is the last stage of the ringdown phase. It implies after the least damped stage the strain will be zero. And, in the least damped stage the second time derivative of strain is zero. The next assumption is to consider it as a sinusoidal wave guided by an exponential decaying function with time.

The signal model used is

$$h(t \geq t_0) = Ae^{-(t-t_0/\tau)}cos2\pi f_0((t-t_0)+\phi_0)$$

In the ringdown phase the remainder hole must "settle down" to the Kerr arrangement which depicts all rotating BH — the "no hair" theorem of general relativity ensures that the Kerr arrangement portrays the last express, regardless of what conditions depict the binary which created it. This "settling down" procedure has been named the ringdown since the waves produced in this age appear as damped sinusoids, like the sound of a struck chime. Truth be told, the quality element Q of dark openings is very low ($Q_{BH} \approx 20$ or thereabouts, contrasted with $Q_{bell} \approx 103 - 105$); when interpreted into sound, one finds that black holes don't ring to such an extent as crash. Ringdown waves "shave" the remainder, guaranteeing that the majority of the "hairness" describing the framework directly after the merger is lost, and what remains is a hairless Kerr black hole.

The ringdown waves comes at frequency

$$f \approx \frac{c^3}{2\pi G(1+z)M}[1 + 0.63(1 - a/M)^{0.3}]$$

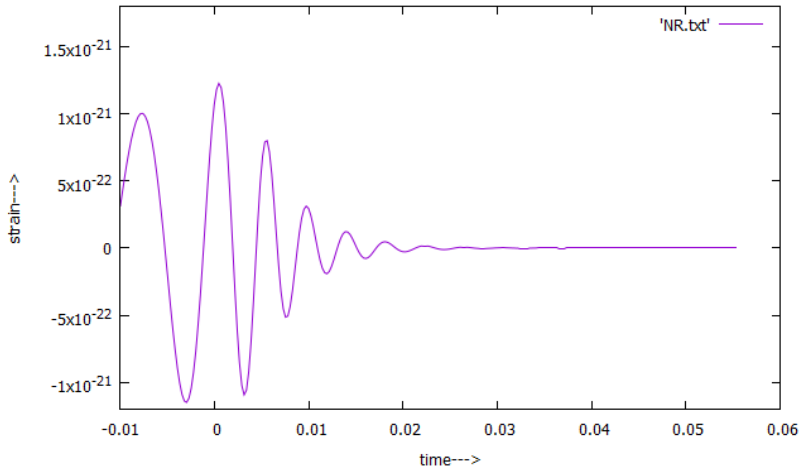

Figure 3.3: The waveform of gravitational wave during the ringdown phase

where z is the cosmological redshift and M is the total mass of the system. For GW150914, $z = 0.09, M = 62M_s$

$$f \approx 1700\frac{10M_s}{(1+z)M}$$

Substituting the values, we get the value of the dominant QNM frequency = 251.55 Hz

3.3 Comparing with the observed waveform

To see whether the value of the aforementioned determined frequency actually holds true or not, we call the signal model equation

$$h(t \geq t_0) = Ae^{-(t-t_0/\tau)}cos2\pi f_0((t - t_0) + \phi_0)$$

Taking $t = t_0 + 0.014$, $\phi_0 = 0, A = 1.21 \times 10^{-21}, \tau = 4$ ms, $f_0 = 251$ Hz

we get the value of the analytically calculated strain $h_{calculated}(t = 0.014) = 8.3 \times 10^{-23}$.

And from the observed waveform we find the observed strain $h_{observed}(t = 0.014) = 8.293 \times 10^{(} - 23)$. Which is the evidence of the triumph of our calculation.

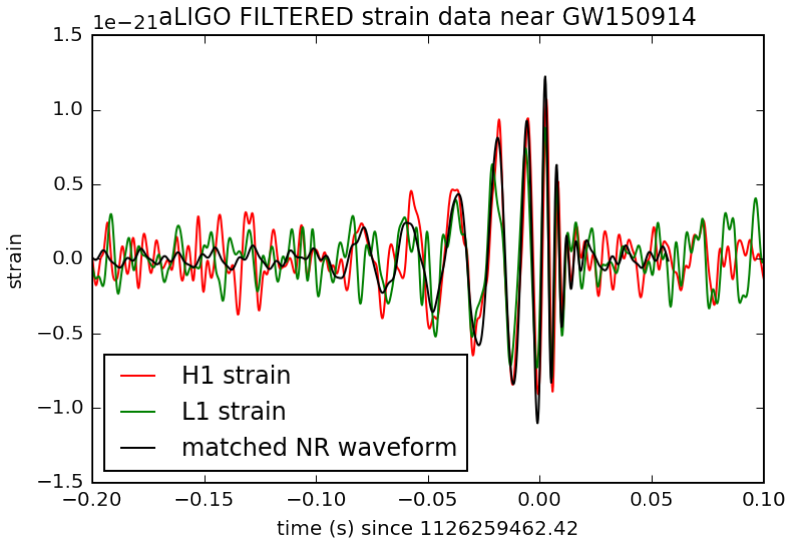

Figure 3.4: The observed waveform as acquired by filtering the strain data from the aLIGO detectors

In the future, this investigation will be extended to two damped sinusoids, and it will minutely investigate the likelihood of autonomously removing the final BH's mass and spin. A trial of the general relativistic no-hair theorem requires the distinguishing proof of no less than two QNM frequencies in the ringdown waveform. Such a test would profit by the perception of a framework with an aggregate mass like the one of GW150914, however with a bigger asymmetry between part masses, which would expand the amplitudes of the sub-dominant modes; a more grounded misalignment of the orbital angular momentum with the viewable pathway would advance enhance their perceivability. At long last, the determination of the remainder mass and spin autonomously of paired segment parameters will permit us to test the second law of black hole dynamics.

Chapter 4

Getting to know to GW from NR and EOB approach

4.1 GW from NR approach

Numerical relativity implies the direct numerical integration of the Einstein field equations, advancing from an "underlying" spacetime to a last state. This requires reconsidering some of our thoughts regarding GR. As a prelude, consider Maxwell's conditions, composed in to some degree non-standard structure:

$\nabla.E = 4\pi\rho; \nabla.B = 0; \frac{\partial E}{\partial t} = -c\nabla \times E; \frac{\partial B}{\partial t} = 4\pi J - c\nabla \times B$

These conditions let us know how E and B are connected all through spacetime. It is noticeable that divergence and curl assume altogether different parts here. The disparity conditions contain no time subsidiaries; on the off chance that we envision "cutting" spacetime into a heap of consistent time cuts, then divergence equations let us know how E and B are obliged on every cut. By contrast, the twist conditions do incorporate time administrators, thus let us know how E and B are connected as we develop from cut to cut. We swing now to forming the Einstein conditions into a structure fitting for advancing from an underlying structure.

4.2 From geometric equations to evolution equations

The Einstein field conditions regularly treat space and time justly. The very question obliges us to change our reasoning: "advancing" from an "underlying" state requires some idea of time. Assume that we have picked a period coordinate, characterising an approach to cut space-time into space and time. We should reformulate the Einstein field conditions utilising amounts characterised exclusively on a given time cut. When time is set, we can openly pick spatial directions in every cut; we indicate x_i on both cuts. Give n a chance to be typical to the base cut. The breach $\alpha = d\tau/dt$ sets the correct time experienced by an eyewitness who moves along n; the movement β_i lets us know by the amount of x_i is dislodged ("moved") on the second cut in respect to the ordinary eyewitness. We will soon see that α_i and β_i are totally unconstrained by Einstein's conditions. They let us set directions as advantageously as could be allowed, summing up the gauge generator utilised as a part of linearised hypothesis to the solid field. The best possible spacetime division of x_i and $x_i + dx_i$ is then

$$ds^2 = -\alpha^2 dt^2 + g_{ij}(dx_i + \beta_i dt)(dx_j + \beta_j dt)$$

(Here, we put c = 1; different variables turn out to be somewhat cumbersome other-wise.) We now have a structure for the metric of spacetime, a thought of steady time cuts, and the typical to a cut n. Since we are keen on comprehension amounts which "live" in a given cut (i.e., orthogonal to the ordinary n), we fabricate the projection tensor $\gamma_\mu = g_\mu + n_\mu n_v$. This tensor is the ideal metric for each slice's geometry. So, coordinates are chosen such that $\gamma_{ti} = \gamma_{tt} = 0$ and $\gamma_{ij} = g_{ij}$.

From Einstein's field equation we get

$$G_\mu = \frac{8\pi G}{T^4} T_{\mu v}$$

Taking this equation and endeavour to project components parallel and orthogonal to $\vec{n}$ yields the component that is completely parallel to $\vec{n}$:

$$G_{\alpha\beta}n^{\alpha}n^{\beta} = 8\pi G T_{\alpha\beta}n^{\alpha}n^{\beta}$$

Which gradually gives rise to $R + K^2 - K_{ij}K^{ij} = 16\pi G\rho$

Here R is the Ricci scalar for the 3 metric $\gamma_{ij,\rho} = T_{\alpha\beta}n^{\alpha}n^{\beta}$ and,

$$K_{ij} = -\gamma_i^{\alpha}\gamma_j^{\beta}\nabla_{\alpha}n_{\beta} = \frac{1}{2\alpha}(-\partial_t + \gamma_i j + D_i\beta_j + D_j\beta_i)$$

is the extraneous curvature. (The operator D_i is a covariant derivative for the metric γ_{ij} .) It portrays the part of the shape which is because of the way that every steady time slice is implanted in the full spacetime. It is known as the Hamiltonian constraint. It contains no time subordinates of K_{ij} . This condition is along these lines a requirement, relating information on a given timeslice. Next, parts parallel to $\vec{n}$ on one index and orthogonal on the other:

$$G_{\alpha\beta}n^{\alpha}\gamma_i^{\beta} = 8\pi G T_{\alpha\beta}n^{\alpha}\gamma_i^{\beta}$$

It gives rise to $D_jK_i^j - D_iK = 8\pi G j_i$. The term matter current $j_i = T_{\alpha\beta}n^{\alpha}\gamma_i^{\beta}$. This equation is actually the momentum constraint since it has no time derivative of K_{ij}.

Ultimately, the projection orthogonal to $\vec{n}$:

$$G_{\alpha\beta}\gamma_i^{\alpha}\gamma_j^{\beta} = 8\pi G T_{\alpha\beta}\gamma_i^{\alpha}\gamma_j^{\beta}$$

giving rise to $\partial_t K_{ij} = -D_iD_j\alpha + \alpha[R_{ij} - 2K_{ik}K_j^k + KK_{ij} - 8\pi G\alpha(matter)] + \beta_k D_k K_{ij} + K_{ik}D_j\beta^k + K_{kj}D_i\beta^k$

The spacetime metric is written as $\tilde{\gamma_{ij}} = e^{-4\phi}\gamma_{ij}$. ϕ is such that $e^{12\phi} = det(\gamma_{ij})$

and $det(\tilde{\gamma_{ij}}) = 1$

The decomposition parts the geometry into "transverse" and "longitudinal" degrees of freedom(epitomised by

$$A_{ij} = K_{ij} - \frac{1}{\gamma_{ij}} K$$

Using $\tilde{A_{ij}} = e^{-4\phi} A_{ij}$ the evolution equations for the aforementioned quantities are determined.

4.3 The EOB approach

Since pN strategies depend on a development in $\phi = GM/rc^2$, it had been believed that they would apply for $r10GM/c^2$, and that numerical relativity would be expected to cover the inspiral past that range, through the last plunge and merger. This reasoning was profoundly changed by Buonanno and Damour (1999), which presented the powerful effective-body approach to deal with two-body elements. This system has turned out to be a fabulous apparatus for depicting the late inspiral, plunge, and merger of two BH.

As the name recommends, the key perception of this methodology is that the movement of two bodies (m1,m2) around each other can view as the movement of a solitary test body of mass $\mu = m_1 m_2/(m_1 + m_2)$ in some spacetime. One starts by looking at the Hamiltonian which gives the moderate commitment to the conditions of movement. Let the binary's momenta be $p_{1,2}$ and its summed up positions $q_{1,2}$. On the off chance that we work in the centre of mass frame, then the Hamiltonian must be a component of the relative position, $q = q_1 - q_2$, and can just depend on the force $p = p_1 = -p_2$. For instance, the traditionalist movement can be depicted to second-post-Newtonian request [i.e., $\mathcal{O}(v^4/c^4)$] with the Hamiltonian

$$H_(q,p) = H_{0(p,q)} + \frac{1}{c^2}H_{2(p,q)} + \frac{1}{c^4}H_{4(p,q)}$$

where $H_{0(p,q)} = |p|^2/2\mu + GM\mu/|q|$ encodes the Newtonian dynamics, and H2,4 depicts pN remedies to that movement. Energy and angular momentum of a binary can be found from this Hamiltonian without an excessive amount of trouble. The following stride is to record an effective one-body metric

$$ds^2 = -A(R)c^2dT^2 + B(R)dR^2 + R^2(d\theta^2 + sin^2\theta d\phi^2)$$

a comparative expression depicts $B(R)$. The coefficients α_i rely on upon diminished mass proportion, $\eta = \mu/M$. The compelling issue is then to portray the movement of a test body in the spacetime . By attesting a correspondence between certain action variables in the pN system and in the compelling structure, the coefficients α_i are totally settled. For instance, one finds that, as η tends to 0, the metric is essentially the Schwarzschild spacetime. The viable issue can hence be viewed as the movement of a test body around a "twisted" BH, with η controlling the distortion.

It is also possible to depict the radiation response in the compelling one-body approach. A key development is to re-aggregate the pN results for vitality misfortune because of GWs keeping in mind the end goal to acquire an outcome that is great into the solid field. In more detail, we put

$$\frac{dp_\phi}{dt} = -\mathcal{F}_\phi$$

The capacity F is known to be in high order in orbital speed v by a mix of investigations in both pN hypothesis It can be composed as

$$\mathcal{F}(v) = \frac{32G}{5c^5}\eta r^4\Omega^5 F(v)$$

where $F(v) = (1 - v/\hat{v})^{-1} P[(1 - v/\hat{v})F(v)]$

The approximate P changes over a N-th request polynomial into a proportion of N/2-th request polynomials whose small v expansion replicates the first polynomial:

$$P[1 + \sum_{n=1}^{N} c_n (v/c)^n] = \frac{1 + \sum_{n=1}^{N/2} d_n (v/c)^n}{1 + \sum_{n=1}^{N/2} e_n (v/c)^n}$$

Utilising this way to deal with characterise the development of a framework because of GW backreaction, it is not all that hard to compute the waves that a binary creates as its individuals winding together. Surely, by enlarging these waves with the "ringdown" that comes once the spacetime is very much depicted by a single black hole, the effective one-body approach has as of late had incredible achievement in coordinating to the waveforms that are delivered by numerical relativity recreations.

4.4 Comparing NR and EOB waveforms

Preceding the breakthrough, the effective one-body approach gave the main solid field portrayal of GWs from the mixture of two BH. Without a doubt, these methods made a somewhat solid expectation: The mixture waveform ought to be genuinely "drilling," as in we expect the frequency and amplitude to trill up to the time when the physical framework is all around displayed as a single distorted/deformed black hole. At that point, it ought to quickly ring down to a quiescent Kerr state. Such a waveform is to be sure precisely what numerical reproductions find, at any rate for the cases that have been concentrated in this way. It has following been found that pre-expressions from the effective one-body formalism give a remarkable portrayal of the outcomes from numerical relativity. There is some opportunity to conform how one matches successful one-body waves to the numerical relativity yield . It gives a case of how well the wave-frames match each other. Over the whole traverse processed, the two waveforms contrast in stage by just a couple of hundredths of

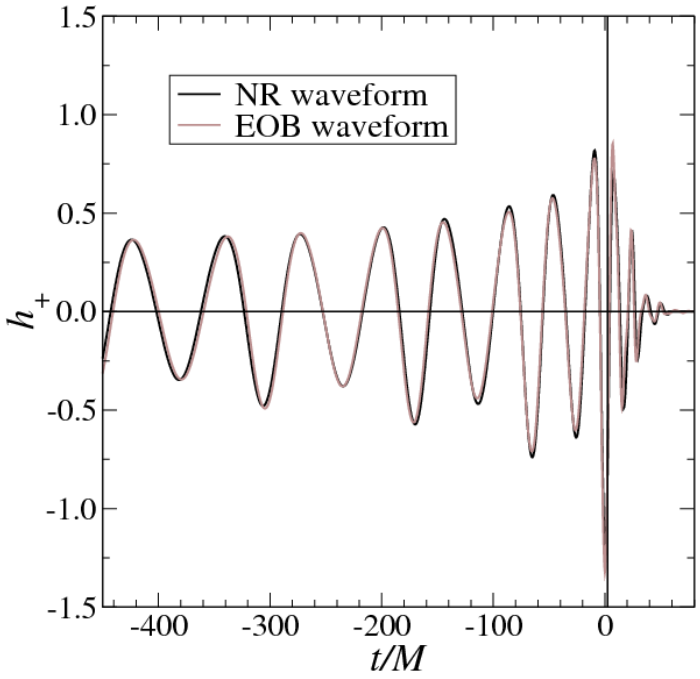

Figure 4.1: The EOB and NR waveforms are getting matched with each other. Since the NR waveform also getss matched with the obsered one. This depicts the success of EOB formalism

a cycle. The understanding is good to the point that one can practically envision "adjusting" the effective one-body waveforms with a moderately little number of expensive numerical relativity calculations, and after that thickly testing the binary parameter space utilising the effective one-body.

Chapter 5

The prediction of low frequency (eLISA) band signal

5.1 Orbital Motion of the Binary Black Holes and Gravitational Wave field

Let us consider that the first BH having mass $m_1 and$ position $r_1(t)$ with respect to the binary system's barycentre, and the velocity be v_1. As for the second BH it has mass $m_2 and$ position $r_2(t)$ with respect to their barycentre and its velocity be v_2.

So the separation vector $r = r_{12} = r_1 - r_2$. So, r_1 and r_2 can be written as follows,

$$r_1 = \frac{m_2}{m} r$$

$$r_2 = -\frac{m_1}{m} r$$

And m $= m_1 + m_2$, the total mass of the binary system which is simply the sum of the two BH. And the velocity relation follows the same rule as before. So, by simply taking the derivatives of the position vectors we get their velocities as follows

$$v_1 = \frac{m_2}{m} v$$

$$v_2 = -\frac{m_1}{m} v$$

And the relative velocity vector $v = v_1 - v_2$

For future usage some relations are introduced $r := |r|$ and $n := |n|$, along with

$$\eta := \frac{m_1 m_2}{(m_1 + m_2)^2}$$

; which is renowned as 'Symmetric mass ratio of the BBH'.

Substituting the quadrupole moment tensor, we get that $I^{jk} = \eta m r^j r^k$ and the virial theorem becomes $\frac{1}{2}\ddot{I} = nm[v^j v^k - (Gm/r)n^j n^k]$ Then we can get

$$h^{jk} = \frac{4Gnm}{c^4 R}[v^j v^k - \frac{Gm}{r} n^j n^k]$$

for the aforementioned binary system created gravitational potential. In order to analyse to whole situation minutely the values of r and v to be determined. In order to analyse the orbital motion, we choose a "orbit-adapted"coordinate system. We choose the coordinate in such a way that its origin coincides with the barycentre of the system , the x-y plane coincides with the orbital plane and the z-axis is on the same direction of the angular momentum vector. Finally the x and y axes align with the orbit's major and minor axes respectively. The Keplerian equations describe the relative orbit as follows

$$r = \frac{p}{1 + e\cos\phi}$$

$$\dot{\phi} = \sqrt{\frac{Gm}{p^3}}(1 + e\cos\phi)^2$$

where ϕ is the 'true anomaly', p is the semi-latus rectum f the orbit and e is the eccentricity. These are the constants of the motion and they are closely related

the to the system's angular momentum and total energy. In the new orbit-adapted coordinates the unit vectors are

$\mathbf{n} = [\cos\phi, \sin\phi, 0]$

$\lambda = [-\sin\phi, \cos\phi, 0]$

These forms a basis in the orbital plane. In terms of these the relative separation and velocity vectors are as follows

$$\mathbf{r} = r\mathbf{n}$$

$$\mathbf{v} = \dot{r}\mathbf{n} + r\dot{\phi}\lambda$$

which complete the description of the motion. Substituting the values of n, λ, ϕ, r the value of h^{jk} becomes

$$h^{jk} = \frac{4\eta}{c^4 R}\frac{(Gm)^2}{p}[(1 + e\cos\phi - e^2\sin^2\phi)n^j n^k + e\sin\phi(1+e\cos\phi)(n^j\lambda^k + \lambda^j n^k) + (1+e\cos\phi)^2\lambda^j\lambda^k]$$

The h^{jk} we determined is the amplitude of the strain of the gravitational waves. But in this chapter we shall only deal with the part where the two black holes are fr apart i.e when the frequency of the gravitational wave is low - during the inspiral phase.

With the help of the aforementioned equation the components of h^{jk} can be easily obtained in the orbital-adapted frame. The motivation of choosing the orbital motion is just to describe the inspiral phase which is said to be most comprehensible phase of the gravitational waves. On the lower frequency range (eLISA band) our classical approximation holds good. So, utilising the previous equation we can easily solve the mystery hidden there.

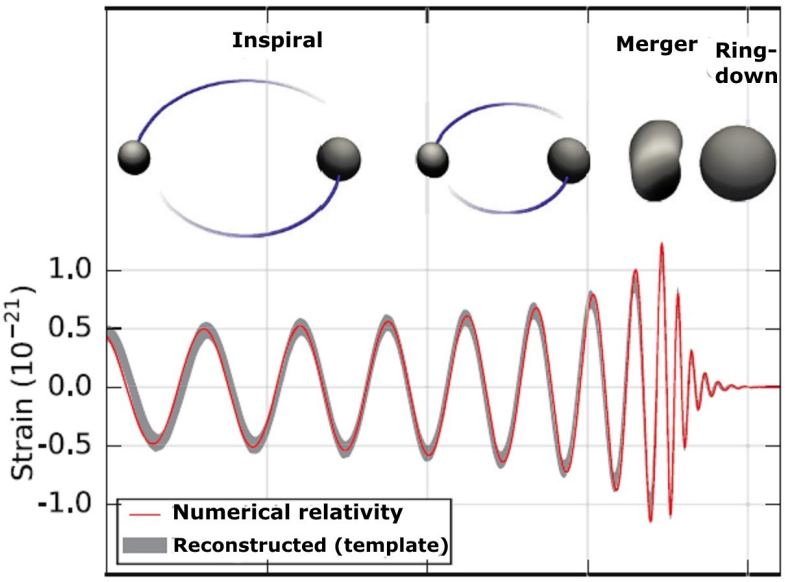

Figure 5.1: Strain of gravitational wave as determined using numerical relativity and reconstructed templates.

5.2 The enigma of the Gravitational Wave polarisation

To determine the gravitational wave polarisations h_+ and $h_\times$, it is essential to introduce a detector-adapted coordinate system (X,Y,Z) in addition to the original coordinate system (x,y,z). The convention of this new coordinate system is as follows. Both this new coordinate system's origin and the origin of the system are coincident. Next, the Z direction points out to the detector at which polarisations are measured. X-Y plane is orthogonal to the Z axis and is also coincident with sky from the detector's point of view. The line of nodes aligns with the X axis, the line at which orbital plane and reference plane meet. X axis is pointed towards the ascending node (by convention). The newly constructed coordinate system looks something like this

$$\mathbf{e}_X = [\cos\omega, -\sin\omega, 0]$$

$$\mathbf{e}_Y = [\cos\iota\sin\omega, \cos\iota\cos\omega, -\sin\iota]$$

$\mathbf{e}_Z = [\sin\iota \sin\omega, \sin\iota \cos\omega, \cos\iota]$

When viewed from this new frame (X,Y,Z), ι, which is the inclination angle is the measurement of the inclination of the orbital plane with respect to the X-Y plane. ω is the 'longitude of pericentre' defined as the angle between the pericentre and the line of nodes. as par as the measurement on the orbital plane. Another angle Ω which called ' The longitude of ascending node' is taken to be 0 by our convention.

We can obtain expressions for the vectors $\mathbf{n}$ and λ. Their expressions are as follows

$\mathbf{n} = [\cos(\omega+\phi), \cos\iota \sin(\omega+\phi), \sin\iota \sin(\omega+\phi)]$

$\lambda = [-\sin(\omega+\phi), \cos\iota \cos(\omega+\phi), \sin\iota \cos(\omega+\phi)]$

The old expressions look like this when expressed in the detector-adapted coordinate system.

Due to the very fact that gravitational waves propagates from the BBH system to the detector along the Z direction e_X and e_Y can be chosen as basis in the transverse subspace. And from this choice the two polarisationsh_+ and $h_\times$ can be calculated as follows

$$h_+ = \frac{1}{2}(e_X^J e_X^k - e_Y^j e_Y^k)h_{jk}$$

$$h_\times = \frac{1}{2}(e_X^J e_Y^k + e_Y^j e_X^k)h_{jk}$$

Substituting all the values manifests that the two polarisations are given by

$$h_+ = h_0 H_+$$

$$h_\times = h_0 H_\times$$

Taking account of the fact that the gravitational wave amplitude h_0 is

$$h_0 = \frac{2\eta}{c^4 R}\frac{(Gm)^2}{p}$$

H_+ = - $(1+\cos^2\iota)[\cos(2\iota+2\omega)+\frac{5}{4}e\cos(\phi+2\omega)+\frac{1}{4}e\cos(3\phi+2\omega)+\frac{1}{2}e^2\cos 2\omega]+\frac{1}{2}e\sin^2\iota(\cos\phi+e)$

$H_\times = 2\cos\iota[\sin(2\iota+2\omega)+\frac{5}{4}e\sin(\phi+2\omega)+\frac{1}{4}e\sin(3\phi+2\omega)+\frac{1}{2}e^2\sin 2\omega]$

These are scale free polarisations.

5.3 The circular orbital motion of the black holes during Inspiral

When the eccentricity(e) is 0 the orbit becomes and ϕ shows a linear increase with time and the rate is $\Omega = \sqrt{\frac{Gm}{p^3}}$ In this case the previous values of the polarisation reduces to

$$H_+ = -(1+\cos^2\iota)\cos 2(\Omega\tau+\omega)$$

$$H_\times = -2\cos\iota\sin 2(\Omega\tau+\omega)$$

5.3.1 Numerical estimation of the amplitude of the strain of GW150914

We can also express the gravitational wave amplitude in terms of the chirp mass

$$M = \eta^{3/5}m = (\frac{m_1^3m_2^3}{m})^{1/5}$$

and the orbital period

$$P := 2\pi\sqrt{\frac{a^3}{Gm}} where$$

a:= p/(1-e^2) is the semi major axis. The expression of the strain amplitude

$$h_0 = \frac{2}{c^4R}(GM)^{5/3}(\frac{2\pi}{P})^{2/3}\frac{1}{1-e^2}$$

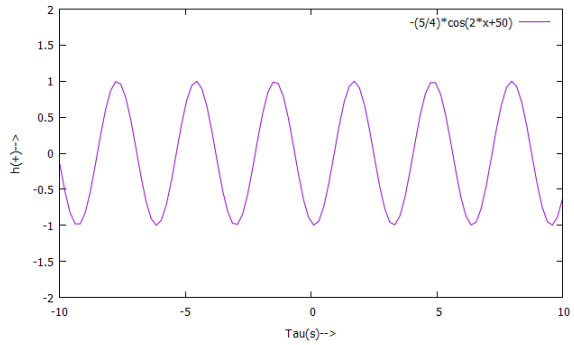

Figure 5.2: The graph of + polarisation of gravitational waves

For GW150914 the masses of the BH are $29M_s$ and $36M_s$,so the chirp mass $M = 64.75M_s$. In the lower frequency range(0.1 mHz- 1 Hz) which is known as the eLISA band, for a particular frequency f = 1 Hz , the orbital period= 1 second and the BBH is at a distance R= 410 Mpc. These numbers finally gives rise to the mathematical value of h_0 which is 3.62 $\times 10^{-22}$.

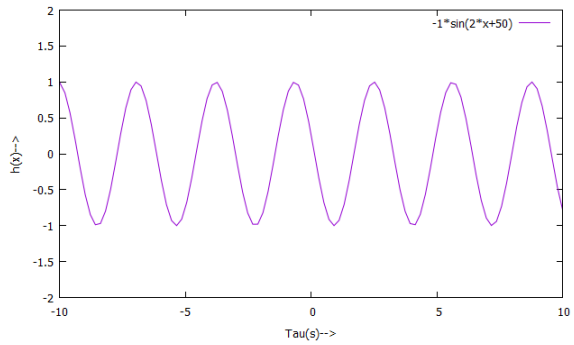

Figure 5.3: The graph of x polarisation of gravitational waves

Chapter 6

Future Work

While this thesis has portrayed the applicability of the LIGO data to analyse the binary black hole merger, its different phases and the low frequency domain; there are so many opportunities in this area which are awaiting for advancement. This section depicts few of the numerous directions.

6.1 Binary Neutron Stars

Gravitational waves are excellent mirror when searching to see the progenitors. Binary neutron stars are a great source of gravitational radiation. So, from the gravitational wave data it is possible to further study them and to comprehend the different phases during they orbiting around each other. It will be a great area of neutron star research to see , how they behave on verge of the formation of gravitational wave; whether there is any change in their accretion power or not.

6.2 Binary Black Holes

GW150914 has been a major breakthrough in the study of binary black holes. From the aLIGO data it will also be possible to portray their formation and evolution.

In addition to that, from the merger waveform, it will also portray their dynamics throughout the process. We can also figure out the dynamics of space-time around them and what affect they have on it.

6.3 Gravitational Wave Astrophysics

The detection of gravitational waves has brought a huge revolution in this domain. First of all, it is the evidence that Einstein's theory of General Relativity' was correct. So, we can further reply on it and advance this domain. Next, LIGO has detected gravitational waves from 43 Hz to 260 Hz. Gravitational waves below and beyond that region has to be discovered. The whole spectrum of gravitational waves will give us a different outlook of the universe. We shall also be able to listen to the gravitational wave burst during the bg bang and get a better idea of the early universe. With gravitational waves we shall be able to make this universe our own laboratory.

Chapter 7

Conclusion

In conclusion it is good to say that this work is a great milestone in the discipline of gravitational wave astronomy. Firstly,the 'Matched Filtering Analysis' technique gives us a significant frequency content in the raw data from which the filtering process clearly manifests the data. Secondly, a blind-burst search has performed here has dealt with finding the astrophysical source, the true burst signal which is a huge advancement. Next, the effective one body formalism has minutely illustrated the merger and the ringdown phase. It has also explained what really happens during that complex phase. In the relativistic black hole motion it is the only model which gets exactly matched with the numerical relativity template which stands for its effectiveness. Furthermore, with the help of a simple model and some mathematics, the dominant QNM ring down frequency determination here has made to visualise the least damped part of the penultimate phase- after which the process almost ceases. It has also dealt with the low frequency gravitational wave by GW150914 where applying simple physics has determined the extremely low strain of gravitational wave in that domain Which clearly points out why the LIGO detectors were unable to sense it. This will be an important contribution on the way to listen to the universe.

Appendix A

Appendix

```
import numpy as np
from scipy import signal
from scipy.interpolate import interp1d
from scipy.signal import butter, filtfilt, iirdesign, zpk2tf, freqz

# the ipython magic below must be commented out in the .py file, since it doesn
#get_ipython().magic(u'matplotlib inline')
#get_ipython().magic(u"config InlineBackend.figure_format = 'retina'")
import matplotlib.pyplot as plt
import matplotlib.mlab as mlab
import h5py

# LIGO-specific readligo.py
import readligo as rl


#-----------------------------------
```

```
#-- Read in data and template
#-------------------------------------
fs = 4096
dataFile = h5py.File('home/mainak/Desktop/GW150914_tutorial/H-H1_LOSC_4_V1-112625
strain_H1, time_H1, chan_dict_H1 = rl.loaddata(dataFile, 'H1')
print '  time_H1: len, min, mean, max = ',    len(time_H1), time_H1.min(), time_H
fs = 4096
# both H1 and L1 will have the same time vector, so:
time = time_H1
# the time sample interval (uniformly sampled!)
dt = time[1] - time[0]
tevent = 1126259462.422          # Mon Sep 14 09:50:45 GMT 2015
deltat = 5.                      # seconds around the event
# index into the strain time series for this time interval:
indxt = np.where((time_H1 >= tevent-deltat) & (time_H1 < tevent+deltat))
data = strain_H1, time_H1, chan_dict_H1
dataFile.close()
time = np.arange(0, 16, 1./fs)

templateFile = h5py.File('/home/mainak/Desktop/GW150914_tutorial/rhOverM_Asymptoti
template = np.array(templateFile['Extrapolated_N4.dir']['Y_l2_m2.dat'])
temp_time = np.arange(0, template.size / (1.0*fs), 1./fs)
templateFile.close()

#------------------------
# Plot data and template
#------------------------
```

```
plt.figure()
plt.plot(time,data)
plt.xlabel('Time (s)')
plt.ylabel('Strain')

plt.figure()
plt.plot(temp_time, template)
plt.xlabel('Time (s)')
plt.ylabel('Strain')
plt.title('Template')

#------------------------
# Plot ASD of data
#------------------------
plt.figure()
power_data, freq_psd = plt.psd(data[12*fs:], Fs=fs, NFFT=fs, visible=False)
plt.close()
plt.figure()
plt.loglog(freq_psd, np.sqrt(power_data), 'b')
plt.xlim([20, 2048])
plt.xlabel('Frequency (Hz)')
plt.ylabel('ASD')
plt.grid('on')

#----------------------
# Plot ASD of template
#----------------------
```

```
power, freq = plt.psd(template, Fs=fs, NFFT=fs, visible=False)
plt.loglog(freq, np.sqrt(power), 'r')
plt.xlabel('Frequency (Hz)')
plt.ylabel('ASD')
plt.grid('on')

#-------------------------------------
# Apply a bandpass filter to the data
#-------------------------------------
(B,A) = sig.butter(4, [80/(fs/2.0), 250/(fs/2.0)], btype='pass')
data_pass= sig.lfilter(B, A, data)
plt.figure()
plt.plot(time, data_pass)
plt.title('Band passed data')
plt.xlabel('Time (s)')

#-----------------------------
# Time domain cross-correlation
#-----------------------------
correlated_raw = np.correlate(data, template, 'valid')
correlated_passed = np.correlate(data_pass, template, 'valid')
plt.figure()
plt.plot(np.arange(0, (correlated_raw.size*1.)/fs, 1.0/fs),correlated_raw)
plt.title('Time domain cross-correlation')
plt.xlabel('Offest between data and template (s)')
plt.figure()
plt.plot(np.arange(0, (correlated_passed.size*1.)/fs, 1.0/fs), correlated_passed)
```

```
plt.xlabel('Offset between data and template (s)')
plt.title('Band passed time domain cross-correlation')

#------------------------------
# Optimal Filter, freq. domain
#------------------------------
#-- Take the FFT of the data
data_fft=np.fft.fft(data)

#--- Pad template and take FFT
zero_pad = np.zeros(data.size - template.size)
template_padded = np.append(template, zero_pad)
template_fft = np.fft.fft(template_padded)

# --- Match FFT frequency bins to PSD frequency bins
datafreq = np.fft.fftfreq(data.size)*fs
power_vec = np.interp(datafreq, freq_psd, power_data)

# --- Apply the optimal matched filter
optimal = data_fft * template_fft.conjugate() / power_vec
optimal_time = 2*np.fft.ifft(optimal)

# -- Normalize the matched filter output
df = np.abs(datafreq[1] - datafreq[0])
sigmasq = 2*(template_fft * template_fft.conjugate() / power_vec).sum() * df
sigma = np.sqrt(np.abs(sigmasq))
SNR = abs(optimal_time) / (sigma)
```

```
# -- Plot the result
plt.figure()
plt.plot(time, SNR)
plt.title('Optimal Matched Filter')
plt.xlabel('Offset time (s)')
plt.ylabel('SNR')
plt.show()
```

A.1 Reference

[1] Thibault Damour. Introductory lectures on the Effective One Body Formalism.

[2] N. Andersson et al. The Transient Gravitational-Wave Sky. Class. Quant. Grav., 30:193002, 2013.

[3] C. L. Fryer and K. C. B. New. Gravitational waves from gravitational collapse. Living Rev. Rel., 14:1, 2011.

[4] E. E. Flanagan and S. A. Hughes. Measuring gravitational waves from binary black hole coalescences: 2. The Waves' information and its extraction, with and without templates. Phys. Rev., D57:4566–4587, 1998.

[5] J. Abadie et al. All-sky search for gravitational-wave bursts in the second joint LIGO-Virgo run. Phys. Rev., D85:122007, 2012. sigma: A Hierarchical Approach. Phys. Rev. Lett., 115(18):181102, 2015.

[6] B. P. Abbott et al. GW150914: First results from the search for binary black hole coalescence with Advanced LIGO. 2016. arXiv:1602.03839.

[7] P. C. Peters. Gravitational Radiation and the Motion of Two Point Masses. Phys. Rev., 136:B1224–B1232, 1964.

[8] B. P. Abbott et al. (LIGO Scientific Collaboration, Virgo Collaboration) (2016), https://dcc.ligo.org/LIGOP1500218/public/main.

[9] A. Einstein, Preuss. Akad. Wiss. Berlin p. 688 (1916).

[10] L. Blanchet, Living Rev. Rel. 17, 2 (2014).

[11] M. Burgay et al., Nature 426, 531 (2003).

[12] N. Wex (2014), arXiv:1402.5594.

[13] C. M. Will, Living Rev. Rel. 17, 4 (2014).

[14] E. Berti et al., Class. Quant. Grav. 32, 243001 (2015).

[15] T. Damour and G. Esposito-Farese, Class. Quant. Grav. 9, 2093 (1992).

[16] P. C. C. Freire et al., Mon. Not. Roy. Astron. Soc. 423, 3328 (2012).

[17] A. Buonanno and T. Damour, Phys. Rev. D 59, 084006 (1999). Mead. A

Simplex M.

[18] Eric Poisson and Clifford M Will, Gravity - Newtonian, Post-Newtonian, Relativistic.

[19] https://losc.ligo.org/s/events/GW150914/GW150914$_t$*utorial.html*

[20] http://einsteintoolkit.org/about/gallery/gw150914/